UC Riverside
2018 Publications

Title
A joint TOA and DOA approach for positioning with LTE signals

Permalink
https://escholarship.org/uc/item/9nt6p88n

Authors
Shamaei, K.
Khalife, J.
Kassas, Z.

Publication Date
2018-04-23

Peer reviewed

A Joint TOA and DOA Approach for Positioning with LTE Signals

Kimia Shamaei, Joe Khalife, and Zaher M. Kassas
Department of Electrical and Computer Engineering
University of California, Riverside, USA
kimia.shamaei@email.ucr.edu,
joe.khalife@email.ucr.edu, zkassas@ieee.org

Abstract—An approach to jointly estimate the time-of-arrival (TOA) and azimuth and elevation angles of the direction-of-arrival (DOA) from received cellular long-term evolution (LTE) signals is developed. The approach uses a uniform planar antenna array and an extended Kalman filter (EKF) to estimate the receiver's position and difference between its clock bias and drift with those of each of the eNodeBs' without any *a priori* knowledge about the receiver's state. Simulation results evaluating the performance of the proposed method are presented for different transmission bandwidths, carrier-to-noise ratios, and number of antennas. Experimental results show an accuracy of 0.55 m in estimating the position of the receiver with real LTE signals.

Keywords—Positioning, localization, navigation, signals of opportunity, LTE, antenna arrays, time-of-arrival, direction-of-arrival.

I. Introduction

Exploiting long-term evolution (LTE) signals – the fourth generation of cellular systems – for navigation has received increased attention recently due to LTE's inherently desirable characteristics: abundance, large transmission bandwidth, high received power, frequency diversity, and geometric favorability of transmitter location [1]–[4]. Network-based positioning capabilities in LTE systems were enabled in Release 9 by introducing the positioning reference signal (PRS). In a network-based approach, the relative timing differences between the received signals from the serving cell and the neighboring cells are transmitted to a location server, where a time-difference-of-arrival (TDOA) approach is used to estimate the position of the user equipment (UE). Network-based positioning approaches suffer from a number of drawbacks: (1) the user's privacy is compromised, since the user's location is revealed to the network [5], (2) localization services are limited only to paying subscribers and from one cellular provider, (3) ambient LTE signals transmitted by other cellular providers are not exploited, and (4) additional bandwidth is required to accommodate the PRS, which caused the majority of cellular providers to choose not to transmit the PRS in favor of dedicating more bandwidth for traffic channels. Due to the aforementioned drawbacks of the network-based approach, alternative UE-based approaches have been studied recently, where several software-defined receivers (SDRs) were proposed to obtain the

time-of-arrival (TOA) of LTE signals [6]–[9]. Experimental results with real and laboratory-emulated LTE signals have demonstrated meter-level navigation accuracy in environments without severe multipath [10], [11].

One of the main challenges in UE-based navigation with LTE signals is the unknown clock biases of the receiver and the base stations (also known as Evolved Node Bs or eNodeBs). Current approaches to overcome this challenge include: (1) estimating and removing the clock bias in a post-processing fashion by using the known position of the UE [10], [12], (2) using perfectly synchronized eNodeBs in laboratory-emulated LTE signals [7], or (3) estimating the difference of the clock biases of the UE and each eNodeB in an extended Kalman filter (EKF) framework [13]. The first approach does not provide an on-the-fly navigation solution in global navigation satellite system (GNSS)-challenged environments. The second approach is not feasible with real LTE signals, whose eNodeBs are not perfectly synchronized. In the third approach, certain *a priori* knowledge about the UE's and/or the eNodeBs' states must be assumed in order to make the estimation problem observable [14]. For example, in [13], the eNodeBs' positions states were assumed to be known as well as the UE's initial states: position, velocity, clock bias, and clock drift. GPS signals were used to estimate the UE's initial states, and such estimates were used to initialize the EKF, which subsequently only used received LTE signals to estimate the UE's position and velocity and the difference between the UE's clock bias and drift and those of the eNodeBs'. However, such initial knowledge about the UE's states might not be available in many practical scenarios, e.g., cold-start in the absence of GNSS signals. To remove the required *a priori* knowledge about the UE's states, a navigation approach is developed, which exploits the temporal diversity of TOA measurements and spatial diversity of direction-of-arrival (DOA) measurements.

The problem of joint angle and delay estimation (JADE) was first addressed in [15], [16], where multiple signal classification (MUSIC) and estimation of signal parameters via rotational invariance techniques (ESPRIT) were used to jointly estimate the delay and angle [17], [18]. MUSIC and ESPRIT are two statistical techniques, which are based on the eigenstructure of the covariance matrix. These algorithms were

obtained based on the assumption of noncoherent received signals. Therefore, in the presence of coherent multipath signals, additional signal processing must be performed [19]. In contrast to the MUSIC and ESPRIT algorithms, the matrix pencil (MP) approach works directly with data and does not need additional signal processing in the presence of coherent multipath signals [20], [21]. The literature on positioning using JADE are either (1) based on simulation results, where the clock bias is not considered [22] or (2) applicable to network-based positioning approaches, where joint TDOA and DOA estimation is used to estimate the UE's position [23]. However, such approaches in the published literature are inapplicable to UE-based positioning with real LTE signals in which neither the UE's or eNodeBs' clock errors are known nor are synchronized.

This paper makes four contributions. First, it develops the first 3-dimensional (3-D) MP approach to jointly estimate the azimuth and elevation angles along with the TOA for LTE signals. Second, it proposes a navigation framework based on joint TOA and DOA to estimate the receiver's position as well as the difference of the clock biases and drifts of the receiver and each eNodeB on-the-fly and without any *a priori* knowledge about the UE's states. Third, it evaluates the effect of the number of antennas, the transmission bandwidth, and the carrier-to-noise ratio (C/N_0) on the estimation error with numerical simulations. Fourth, it presents the first experimental demonstration of positioning with LTE signals without *a priori* knowledge about the UE's states via the joint TOA and DOA estimation framework developed in this paper. The experimental results show a UE positioning estimation error of 0.55 m with the proposed framework.

The remainder of this paper is organized as follows. Section II describes the LTE signal model and the ranging signals. Section III discusses the received signal model. Section IV presents the 3-D MP algorithm to jointly estimate the TOA and DOA for LTE signals. Section V discusses the navigation framework to estimate the receiver's position and the difference of the clock biases and drifts of the receiver and each eNodeB. Section VI presents simulation results evaluating the effect of the number of antennas, transmission bandwidth, and C/N_0 on the estimation error. Section VII presents the experimental results. Concluding remarks are discussed in Section VIII.

II. TRANSMITTED SIGNAL MODEL

In LTE downlink transmission, orthogonal frequency division multiplexing (OFDM) is used to transmit the data. An OFDM symbol is obtained by parallelizing the serial data symbols into groups of length N_r, zero-padding to length N_c, and taking an inverse fast Fourier transform (IFFT). To suppress the interference due to multipath, the last L_{CP} elements of each symbol are repeated at the beginning, namely the cyclic prefix (CP). Each symbol has a duration of $T_{symb} = 1/\Delta f$, where $\Delta f = 15$ KHz is the subcarrier spacing. In LTE systems, the values of N_r and N_c, which are directly related to the bandwidth, can only accept the values presented in Table I

Bandwidth (MHz)	Total number of subcarriers (N_c)	Number of subcarriers used (N_r)
1.4	128	72
3	256	180
5	512	300
10	1024	600
15	1536	900
20	2048	1200

[24]. An LTE frame has a duration of 10 ms and is composed of 20 slots, each of which contains 7 OFDM symbols.

There are three types of reference signals broadcast in every LTE frame that can be exploited for TOA- and DOA-based navigation purposes: (1) the primary synchronization signal (PSS), (2) the secondary synchronization signal (SSS), and (3) the cell-specific reference signal (CRS). The PSS and SSS are mainly transmitted to provide the frame start time and the eNodeB's cell ID to the UE. The PSS is a Zadoff-Chu sequence of length 62 and is transmitted on the last symbols of slots 0 and 10. The PSS is transmitted in one form of three possible sequences, each of which maps to the integer $N_{ID}^{(2)} \in \{0, 1, 2\}$ representing the sector ID of the eNodeB.

The SSS is an orthogonal sequence of length 62 and is transmitted on the sixth symbol of slot 0 or 10. This orthogonal sequence is defined based on $N_{ID}^{(2)}$ and the slot number in which the SSS is transmitted. The SSS is transmitted in one of 168 possible forms, each of which maps to the integer $N_{ID}^{(1)} \in \{0, \cdots, 167\}$ representing the eNodeB's group identifier. By knowing $N_{ID}^{(1)}$ and $N_{ID}^{(2)}$, the UE can obtain the eNodeB's cell ID according to [24]

$$N_{ID}^{Cell} = 3 \times N_{ID}^{(1)} + N_{ID}^{(2)}.$$

The CRS, which is scattered in time and bandwidth, is transmitted for channel estimation purposes. The CRS is an orthogonal sequence that is defined based on the cell ID, the allocated symbol number, the slot number, and the transmission antenna port number. The eNodeB's cell ID indicates the subcarriers designated for the CRS [25].

The UE first correlates the received LTE signal with the locally generated PSS and SSS to estimate the frame start time. Next, the CP is removed and a fast Fourier transform (FFT) is taken to convert the signal to the frame structure. Then, the receiver estimates the channel frequency response by wiping off the locally generated CRS from the received signal. Finally, the estimated channel frequency response is used to estimate the TOA and DOA of the received signal.

III. RECEIVED SIGNAL MODEL

An antenna array can be used to estimate the DOA of the received signal from the phase difference of the received signal in different antenna elements. The literature on signal processing of antenna arrays describes the array propagation vector for different antenna array structures [26]. One simple

array structure is the uniform linear array (ULA), where the antenna elements are separated equally in a linear form, as shown in Fig. 1. The estimated DOA using a ULA is always in the interval of $[0, \pi]$. This will introduce an ambiguity in the DOA estimates since signals received at angles $\theta \in [0, \pi]$ and $-\theta$ will be measured as θ. Due to this ambiguity, a uniform planer array (UPA) is used in this paper to estimate the azimuth and elevation angles of the received signal without introducing any ambiguities in the DOA estimate.
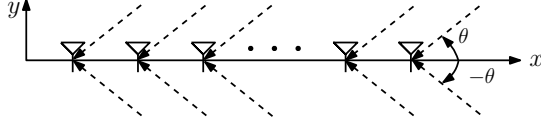

Fig. 1. ULA structure and DOA representation

Fig. 2 shows the antenna array of the receiver, which is assumed to be a UPA with M antenna elements in the x-direction and N antenna elements in the y-direction. The distance between adjacent antenna elements is typically assigned to be $d = \lambda/2$, where $\lambda = c/f_c$ is the received signal wavelength, c is the speed-of-light, and f_c is the carrier frequency. The transmitted signal from the u-th eNodeB propagates to the antenna array through $L^{(u)}$ different paths, where the l-th arriving path impinges the antenna array at an azimuth angle $\phi_l^{(u)}$ and an elevation angle $\theta_l^{(u)}$, as shown in Fig. 2. Therefore, the impulse response of the channel between the u-th eNodeB and the (m, n)-th antenna element and for the k-th subcarrier can be expressed as

$$h_{m,n}^{(u)}(t) = \sum_{l=0}^{L^{(u)}-1} \alpha_l^{(u)} a_{m,n}\left(\phi_l^{(u)}, \theta_l^{(u)}\right) \delta\left(t - \tau_l^{(u)}\right), \quad (1)$$

$$\text{for} \quad m = 0, \cdots, M-1, \quad \text{and} \quad n = 0, \cdots, N-1,$$

where $\alpha_l^{(u)}$ and $\tau_l^{(u)}$ are the attenuation and the delay of the l-th path, respectively, $a_{m,n}\left(\phi_l^{(u)}, \theta_l^{(u)}\right)$ is the (m, n)-th antenna response to l-th multipath, which for a UPA can be shown to be

$$a_{m,n}\left(\phi_l^{(u)}, \theta_l^{(u)}\right) = e^{j\frac{2\pi f_k md\sin\left(\theta_l^{(u)}\right)\cos\left(\phi_l^{(u)}\right)}{c}}$$

$$e^{j\frac{2\pi f_k nd\sin\left(\theta_l^{(u)}\right)\sin\left(\phi_l^{(u)}\right)}{c}},$$

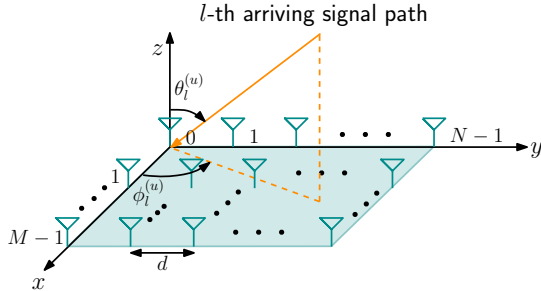where f_k is the k-th subcarrier transmission frequency [23].

Fig. 2. UPA structure and DOA representation

The received signal from the u-th eNodeB at the (m, n)-th antenna element can be obtained as

$$r_{m,n}^{(u)}(t) = h_{m,n}^{(u)}(t) * y^{(u)}(t) + w_{m,n}(t),$$

where $*$ represents the convolution operation, $y^{(u)}(t)$ is the transmitted signal from the u-th eNodeB, and $w_{m,n}(t)$ is the measurement noise, which is modeled as an additive white Gaussian process.

At the receiver side, the received signal is first sampled at a sampling interval $T_s = T_{symb}/N_c$. Next, a coarse estimate of the frame start time is obtained using the PSS and SSS correlations [27]. Then, the CP is removed and an FFT is taken, yielding

$$R_{m,n}^{(u)}(k) = H_{m,n}^{(u)}(k)Y^{(u)}(k) + W_{m,n}(k),$$

$$\text{for} \quad k = 0, \cdots, N_c - 1,$$

where $H_{m,n}^{(u)}(k)$ is the complex-valued channel frequency response (CFR) at the k-th subcarrier and $Y^{(u)}(k)$ and $W_{m,n}(k)$ are the FFT of the transmitted signal and noise, respectively. In LTE systems, the CRS is scattered on the subcarriers of multiple transmitted symbols in every frame; therefore, the transmitted symbols containing the CRS can be modeled as

$$Y^{(u)}(k) = \begin{cases} S^{(u)}(k), & \text{if } k \in N_{CRS}^{(u)}, \\ D^{(u)}(k), & \text{otherwise}, \end{cases}$$

where $S^{(u)}(k)$ represents the CRS sequence and $D^{(u)}(k)$ represents some other data signals; $N_{CRS}^{(u)}$ denotes the set of subcarriers containing the CRS; $N_{CRS}^{(u)} = q\Delta_{CRS} + \nu_{N_{ID}^{Cell}}$ for $q = 0, \cdots, N_s - 1$ in the symbols containing the CRS; $N_s = \lfloor N_r/\Delta_{CRS} \rfloor$ and $\Delta_{CRS} = 6$; and $\nu_{N_{ID}^{Cell}}$ is a constant shift, which is a function of the symbol number, transmission antenna port number, and the cell ID.

By knowing $S^{(u)}(k)$ at the receiver, the CFR of the (m, n)-th antenna element for the k-th subcarrier is estimated according to

$$\hat{H}_{m,n}^{(u)}(k) = R_{m,n}^{(u)}(k)S^{(u)^*}(k),$$

where $(\cdot)^*$ denotes the complex conjugate operations. The estimated CFR $\hat{H}_{m,n}^{(u)}(k)$ can be modeled as

$$\hat{H}_{m,n}^{(u)}(k) = \sum_{l=0}^{L^{(u)}} \alpha_l^{(u)} e^{-j\omega_c \tau_l^{(u)}} \quad (2)$$

$$\cdot e^{j\omega_c md\sin\left(\theta_l^{(u)}\right)\cos\left(\phi_l^{(u)}\right)/c} \quad (3)$$

$$\cdot e^{j\omega_c nd\sin\left(\theta_l^{(u)}\right)\sin\left(\phi_l^{(u)}\right)/c} \quad (4)$$

$$\cdot e^{-j2\pi k\Delta f\left(\tau_l^{(u)} + \Delta\tau\right)} + V_{m,n}(k), \quad (5)$$

$$\text{for} \quad k = q\Delta_{CRS} + \nu_{N_{ID}^{Cell}}, \quad \text{and} \quad q = 0, \cdots, N_s - 1, \quad (6)$$

where $\omega_c = 2\pi f_c$, $V_{m,n}(k) \triangleq W_{m,n}(k)S^{(u)^*}(k)$, and

$$\Delta\tau = \left[m\sin\left(\theta_l^{(u)}\right)\cos\left(\phi_l^{(u)}\right) + n\sin\left(\theta_l^{(u)}\right)\sin\left(\phi_l^{(u)}\right)\right] d/c.$$

In practical scenarios, the time delay $\tau_l^{(u)}$ due to the propagation path between the eNodeB and the UE is significantly

higher than the time delay due to the array structure $\Delta\tau$. Therefore, $\Delta\tau$ is ignored. The matrix $\bar{\mathbf{H}}^{(u)}$ can be constructed with the elements $\bar{H}^{(u)}(m,n,q)$ defined as

$$\bar{H}^{(u)}(m,n,q) \triangleq \hat{H}_{m,n}^{(u)}(k)$$
$$\approx \sum_{l=0}^{L^{(u)}} \beta_l\, x_l^m y_l^n z_l^q + V_{m,n}(k), \tag{7}$$

$$\text{for} \quad k = q\Delta_{CRS} + \nu_{N_{ID}^{Cell}}, \quad \text{and} \quad q = 0,\cdots,N_s-1,$$

where

$$\beta_l \triangleq \alpha_l^{(u)} e^{-j\omega_c \tau_l^{(u)}} e^{-j2\pi\nu_{N_{ID}^{Cell}}\Delta f \tau_l^{(u)}},$$
$$x_l^{(u)} \triangleq e^{j\omega_c d \sin\theta_l^{(u)} \cos\phi_l^{(u)}/c},$$
$$y_l^{(u)} \triangleq e^{j\omega_c d \sin\theta_l^{(u)} \sin\phi_l^{(u)}/c},$$
$$z_l^{(u)} \triangleq e^{-j2\pi\Delta f \Delta_{CRS}\tau_l^{(u)}}.$$

The objective is to estimate $(x_l^{(u)}, y_l^{(u)}, z_l^{(u)})$ and obtain the relative TOA and DOA of each path as

$$\hat{\theta}_l^{(u)} = \sin^{-1}\left(\sqrt{G^2+E^2}\right), \tag{8}$$

$$\hat{\phi}_l^{(u)} = \text{atan2}\left(E, G\right), \tag{9}$$

$$\hat{\tau}_l^{(u)} = -\frac{1}{2\pi\Delta f \Delta_{CRS}}\text{atan2}\left(\Im\left\{\hat{z}_l^{(u)}\right\}, \Re\left\{\hat{z}_l^{(u)}\right\}\right), \tag{10}$$

where atan2 is the four-quadrant inverse tangent function, $\Re\{\cdot\}$ and $\Im\{\cdot\}$ denote the real and imaginary parts, respectively, and

$$G = \frac{c}{\omega_c d}\text{atan2}\left(\Im\left\{\hat{x}_l^{(u)}\right\}, \Re\left\{\hat{x}_l^{(u)}\right\}\right),$$
$$E = \frac{c}{\omega_c d}\text{atan2}\left(\Im\left\{\hat{y}_l^{(u)}\right\}, \Re\left\{\hat{y}_l^{(u)}\right\}\right).$$

IV. JOINT TOA AND DOA ESTIMATION

In this section, the 3-D MP algorithm to jointly estimate the TOA and DOA in LTE systems is first presented. Then, the pairing approach is discussed, which is used to pair the estimated TOAs with their corresponding elevations and azimuths angles. For simplicity of notations, the superscript (u), which denotes the u-th eNodeB, will be omitted in this section.

A. TOA and DOA Estimation

A 3-D MP algorithm is divided into three 1-D MP algorithms to estimate x_l, y_l, and z_l individually [21], [28]. The 3-D MP algorithm has five main steps that are discussed in this subsection.

Step 1: Construct the enhanced-matrix as

$$\mathbf{X}_e = \begin{bmatrix} \mathbf{D}_0 & \mathbf{D}_1 & \cdots & \mathbf{D}_{N_s-R} \\ \mathbf{D}_1 & \mathbf{D}_2 & \cdots & \mathbf{D}_{N_s-R+1} \\ \vdots & \vdots & \ddots & \vdots \\ \mathbf{D}_{R-1} & \mathbf{D}_R & \cdots & \mathbf{D}_{N_s-1} \end{bmatrix}_{PKR\times[(M-P+1)}, \\ {}_{(N-K+1)(N_s-R+1)]}$$

where

$$\mathbf{D}_z = \begin{bmatrix} \mathbf{D}_{0,z} & \mathbf{D}_{1,z} & \cdots & \mathbf{D}_{N-K,z} \\ \mathbf{D}_{1,z} & \mathbf{D}_{2,z} & \cdots & \mathbf{D}_{N-K+1,z} \\ \vdots & \vdots & \ddots & \vdots \\ \mathbf{D}_{K-1,z} & \mathbf{D}_{K,z} & \cdots & \mathbf{D}_{N-1,z} \end{bmatrix}, z=0,1,\ldots,N_s-1,$$

$$\mathbf{D}_{y,z} =$$
$$\begin{bmatrix} \bar{H}(0,y,z) & \bar{H}(1,y,z) & \cdots & \bar{H}(M-P,y,z) \\ \bar{H}(1,y,z) & \bar{H}(2,y,z) & \cdots & \bar{H}(M-P+1,y,z) \\ \vdots & \vdots & \ddots & \vdots \\ \bar{H}(P-1,y,z) & \bar{H}(P,y,z) & \cdots & \bar{H}(M-1,y,z) \end{bmatrix},$$

where $y = 0,1,\ldots,N-1$; K, P, and R are pencil parameters. The pencil parameters are tuning parameters that are used to improve the estimation accuracy and must satisfy the following necessary conditions

$$(P-1)RK \geq L,$$
$$(K-1)PK \geq L,$$
$$(R-1)PK \geq L,$$
$$(M-P+1)(N-K+1)(N_s-R+1) \geq L.$$

It is worth mentioning that increasing the pencil parameters will increase the computational cost. Therefore, there is a trade-off between the achievable accuracy and the computational cost.

Step 2: Decompose $\mathbf{X}_e$ using the singular-value decomposition (SVD) as

$$\mathbf{X}_e = \mathbf{U}\boldsymbol{\Sigma}\mathbf{V}^{\mathsf{H}},$$

where the superscript H denotes the Hermitian transpose, $\mathbf{U}$ and $\mathbf{V}$ are unitary matrices, and $\boldsymbol{\Sigma}$ is a diagonal matrix of singular values $\sigma_1 \geq \cdots \geq \sigma_{KPR}$. Next, use the minimum description length (MDL) criterion to estimate the multipath channel length $L^{(u)}$ as

$$MDL(i) = -(d_1-i)\,d_2\ln\left\{\frac{\prod_{n=i+1}^{d_1}\lambda_n^{1/(d_1-i)}}{\frac{1}{d_1-i}\sum_{n=i+1}^{d_1}\lambda_n}\right\}$$
$$+ \frac{1}{2}i\,(2\,d_1-i)\ln(d_2),$$
$$\text{for} \quad i=0,\cdots,d_1-1,$$

where $d_1 = KPR$, $d_2 = (M-P+1)(N-K+1)(N_s-R+1)$, and $\lambda_n = \sigma_n^2/d_2$ [29]. The value of i that minimizes $MDL(i)$ determines the estimate of L. Note that KPR must be large enough to include the signal and noise subspaces; however, it should be less than $(M-P+1)(N-K+1)(N_s-P+1)$ to reduce the computational complexity [23].

Step 3: Form $\mathbf{U}_s$ as the submatrix of $\mathbf{U}$ corresponding to the $\hat{L}$ largest singular values. Build matrices $\mathbf{U}_{s_1}$ and $\mathbf{U}_{s_2}$ as

$$\mathbf{U}_s = \begin{bmatrix} \mathbf{U}_{s_1} \\ \text{last } PK \text{ rows} \end{bmatrix} = \begin{bmatrix} \text{first } PK \text{ rows} \\ \mathbf{U}_{s_2} \end{bmatrix}. \tag{11}$$

Derive the generalized eigenvalues of the pencil pair $(\mathbf{U}_{s_2}, \mathbf{U}_{s_1})$, which are equal to the eigenvalues of $\boldsymbol{\Psi}_z =$

$\mathbf{U}_{s_1}^{\dagger}\mathbf{U}_{s_2}$, where $\dagger$ denotes Moore-Penrose pseudo-inverse. The resulting eigenvalues are $\left\{\hat{z}_{i_{z,1}},\cdots,\hat{z}_{i_{z,\hat{L}}}\right\}$, which is a permutation of the vector $\{\hat{z}_1,\cdots,\hat{z}_{\hat{L}}\}$. Subsection IV-B discusses how to properly reorder the vector $\left\{\hat{z}_{i_{z,1}},\cdots,\hat{z}_{i_{z,\hat{L}}}\right\}$.

Step 4: Form the matrix $\mathbf{U}_{sj} = \mathbf{J}\mathbf{U}_s$, where $\mathbf{J}$ is the permutation matrix defined as

$$\mathbf{J} \triangleq [\mathbf{S}(0),\mathbf{S}(1),\cdots,\mathbf{S}(K-1)]^{\mathsf{T}},$$

where the superscript T denotes the transpose operator and $\mathbf{S}(i)$ is defined as

$$\begin{aligned}\mathbf{S}(i) = [&\boldsymbol{p}(1+iP),\cdots,\boldsymbol{p}(P+iP),\\ &\boldsymbol{p}(1+iP+PK),\cdots,\boldsymbol{p}(P+iP+PK),\cdots\cdots,\\ &\boldsymbol{p}(1+iP+(R-1)PK),\cdots,\boldsymbol{p}(P+iP+(R-1)PK)],\end{aligned}$$

where $\boldsymbol{p}(\ell)$ is a column vector of size KPR with one in the (ℓ)-th element and zero elsewhere. Build $\mathbf{U}_{sj_1}$ and $\mathbf{U}_{sj_2}$ from $\mathbf{U}_{sj}$ by removing the last and first PR rows, similar to (11). The eigenvalues of $\boldsymbol{\Psi}_y = \mathbf{U}_{sj_1}^{\dagger}\mathbf{U}_{sj_2}$ are $\left\{\hat{y}_{i_{y,1}},\cdots,\hat{y}_{i_{y,\hat{L}}}\right\}$, which is a permutation of the vector $\{\hat{y}_1,\cdots,\hat{y}_{\hat{L}}\}$. Subsection IV-B discusses how to properly reorder the vector $\left\{\hat{y}_{i_{y,1}},\cdots,\hat{y}_{i_{y,\hat{L}}}\right\}$.

Step 5: Form matrix $\mathbf{U}_{sp} = \mathbf{P}\mathbf{U}_s$, where $\mathbf{P}$ is the permutation matrix defined as

$$\begin{aligned}\mathbf{P} \triangleq [&\boldsymbol{p}(1),\boldsymbol{p}(1+P),\cdots,\boldsymbol{p}(1+(KR-1)P),\\ &\boldsymbol{p}(2),\boldsymbol{p}(2+P),\cdots,\boldsymbol{p}(2+(KR-1)P),\cdots\cdots,\\ &\boldsymbol{p}(P),\boldsymbol{p}(P+P),\cdots,\boldsymbol{p}(P+(KR-1)P)]^{\mathsf{T}},\end{aligned}$$

Build $\mathbf{U}_{sp_1}$ and $\mathbf{U}_{sp_2}$ from $\mathbf{U}_{sp}$ by removing the last and first KR rows, similar to (11). The eigenvalues of $\boldsymbol{\Psi}_x = \mathbf{U}_{sp_1}^{\dagger}\mathbf{U}_{sp_2}$ are $\left\{\hat{x}_{i_{x,1}},\cdots,\hat{x}_{i_{x,\hat{L}}}\right\}$, which is a permutation of the vector $\{\hat{x}_1,\cdots,\hat{x}_{\hat{L}}\}$. Subsection IV-B discusses how to properly reorder the vector $\left\{\hat{x}_{i_{x,1}},\cdots,\hat{x}_{i_{x,\hat{L}}}\right\}$.

B. Pairing

Steps 1–5 in Subsection IV-A showed how to estimate $\left\{\hat{x}_{i_{x,1}},\cdots,\hat{x}_{i_{x,\hat{L}}}\right\}$, $\left\{\hat{y}_{i_{y,1}},\cdots,\hat{y}_{i_{y,\hat{L}}}\right\}$, and $\left\{\hat{z}_{i_{z,1}},\cdots,\hat{z}_{i_{z,\hat{L}}}\right\}$ individually. These estimates are not necessarily in the same order. Therefore, they must be paired together correctly before calculating the TOA and DOA.

It can be shown that $\boldsymbol{\Psi}_x$, $\boldsymbol{\Psi}_y$, and $\boldsymbol{\Psi}_z$ have the same eigenvectors, which implies

$$\begin{aligned}\boldsymbol{\Psi}_x &= \mathbf{A}\mathbf{X}\mathbf{A}^{-1},\\ \boldsymbol{\Psi}_y &= \mathbf{A}\mathbf{Y}\mathbf{A}^{-1},\\ \boldsymbol{\Psi}_z &= \mathbf{A}\mathbf{Z}\mathbf{A}^{-1},\end{aligned}$$

where $\mathbf{X} \triangleq \text{diag}\{\hat{x}_{i_{x,1}},\cdots,\hat{x}_{i_{x,\hat{L}}}\}$, $\mathbf{Y} \triangleq \text{diag}\{\hat{y}_{i_{y,1}},\cdots,\hat{y}_{i_{y,\hat{L}}}\}$, and $\mathbf{Z} \triangleq \text{diag}\{\hat{z}_{i_{z,1}},\cdots,\hat{z}_{i_{z,\hat{L}}}\}$. Next, the eigenvalues of $\boldsymbol{\Psi}_z$, i.e., $\left\{\hat{z}_{i_{z,1}},\cdots,\hat{z}_{i_{z,\hat{L}}}\right\}$, are used to calculate the TOA of each multipath, resulting in the TOA estimates $\left\{\hat{\tau}_{z,i_1},\ldots,\hat{\tau}_{z,i_{\hat{L}}}\right\}$. Next, the TOA estimates are

sorted in ascending order, yielding the vector $\{\hat{\tau}_1,\ldots,\hat{\tau}_{\hat{L}}\}$. The eigenvectors of $\boldsymbol{\Psi}_z$, which are the column vectors of matrix $\mathbf{A}$, must be also sorted according to the TOA estimates, yielding the matrix $\mathbf{A}'$. Then, define the matrices $\mathbf{X}'$ and $\mathbf{Y}'$ according to

$$\begin{aligned}\mathbf{X}' &= \mathbf{A}'^{-1}\boldsymbol{\Psi}_x\mathbf{A}',\\ \mathbf{Y}' &= \mathbf{A}'^{-1}\boldsymbol{\Psi}_y\mathbf{A}'.\end{aligned}$$

The diagonal elements of $\mathbf{X}'$ and $\mathbf{Y}'$ are $\{\hat{x}_1,\cdots,\hat{x}_{\hat{L}}\}$ and $\{\hat{y}_1,\cdots,\hat{y}_{\hat{L}}\}$, respectively. Note that $\{\hat{x}_1,\cdots,\hat{x}_{\hat{L}}\}$, $\{\hat{y}_1,\cdots,\hat{y}_{\hat{L}}\}$, and $\{\hat{z}_1,\cdots,\hat{z}_{\hat{L}}\}$ are now in the right order.

C. LOS TOA and DOA Estimation

The vectors $\{\hat{x}_1,\cdots,\hat{x}_{\hat{L}}\}$, $\{\hat{y}_1,\cdots,\hat{y}_{\hat{L}}\}$, and $\{\hat{z}_1,\cdots,\hat{z}_{\hat{L}}\}$ are used in (8)–(10) to obtain TOA and DOA estimates captured by the vectors $\{\hat{\tau}_1,\ldots,\hat{\tau}_{\hat{L}}\}$, $\left\{\hat{\theta}_1,\ldots,\hat{\theta}_{\hat{L}}\right\}$, and $\left\{\hat{\phi}_1,\ldots,\hat{\phi}_{\hat{L}}\right\}$. The TOA and DOA estimates used by the navigation filter pertain to the LOS path, which are now the first elements of the TOA and DOA estimates. Therefore, define the estimated LOS TOA and DOA measurements as

$$\hat{\tau}_{LOS} \triangleq \hat{\tau}_1, \quad \hat{\theta}_{LOS} \triangleq \hat{\theta}_1, \quad \text{and} \quad \hat{\phi}_{LOS} \triangleq \hat{\phi}_1.$$

Remark The MDL criterion tends to overestimate the channel length. Therefore, the LOS TOA and DOA estimates may contain outliers. A median filter can be used to remove these outliers.

V. NAVIGATION FRAMEWORK

A. TOA and DOA Measurement Models

Section IV discussed how TOA and DOA can be jointly estimated using the 3-D MP algorithm. By multiplying the estimated LOS TOAs for all eNodeBs by c, pseudorange measurements can be obtained, namely

$$\rho^{(u)} = c\,\hat{\tau}_{LOS}^{(u)}, \quad u = 0,\cdots,U-1,$$

where $\hat{\tau}_{LOS}^{(u)}$ is the estimated LOS TOA from the u-th eNodeB and U is the total number of eNodeBs in the environment.

The pseudorange can be modeled in terms of the receiver's and eNodeBs' states as

$$\rho^{(u)} = r^{(u)} + c\left(\delta t_r - \delta t_s^{(u)}\right) + v_\rho^{(u)}, \quad u = 0,\cdots,U-1,$$

where $r^{(u)} = \left\|\boldsymbol{r}_r - \boldsymbol{r}_s^{(u)}\right\|_2$ is the range between the receiver and the u-th eNodeB; $\boldsymbol{r}_r = [x_r,y_r,z_r]^{\mathsf{T}}$ is the receiver's 3–D position; $\boldsymbol{r}_s^{(u)} = \left[x_s^{(u)},y_s^{(u)},z_s^{(u)}\right]^{\mathsf{T}}$ is the u-th eNodeB's 3–D position; δt_r and $\delta t_s^{(u)}$ are the receiver's and u-th eNodeB's clock biases, respectively; and $v_\rho^{(u)}$ is the measurement noise, which is modeled as a zero-mean Gaussian random variable with standard deviation $\sigma_\rho^{(u)}$.

The estimated LOS DOA measurements for each eNodeB can be modeled in terms of the receiver's and eNodeBs' states as

$$\hat{\theta}_{LOS}^{(u)} = \cos^{-1}\left[\frac{z_s^{(u)} - z_r}{r^{(u)}}\right] + v_\theta^{(u)},$$

$$\hat{\phi}_{LOS}^{(u)} = \text{atan2}\left(y_s^{(u)} - y_r, x_s^{(u)} - x_r\right) + v_\phi^{(u)},$$

$$\text{for} \quad u = 0, \cdots, U - 1,$$

where $v_\theta^{(u)}$ and $v_\phi^{(u)}$ are the DOA measurement noises, which are modeled as a zero-mean Gaussian random variables with standard deviations $\sigma_\theta^{(u)}$ and $\sigma_\phi^{(u)}$, respectively.

Note that the receiver's range to the u-th eNodeB $r^{(u)}$ is typically significantly higher than the difference of the height of the eNodeBs and the receiver $z_s^{(u)} - z_r$. Therefore, in LTE systems, $\theta_{LOS}^{(u)}$ is usually around $\pi/2$. Since $\theta_{LOS}^{(u)}$ is obtained using an inverse sine function (cf. (8)) and an inverse sine function's slope is high for $\theta_{LOS}^{(u)} \approx \pi/2$, the estimation error for $\theta_{LOS}^{(u)}$ can be significantly high. Therefore, only the azimuth angle $\phi_{LOS}^{(u)}$ is used as the DOA measurement in this paper, and only the 2-D position of the receiver is estimated. The receiver's altitude can be obtained using other sensors (e.g., barometer).

It has been previously shown that the eNodeBs' positions can be mapped with a high degree of accuracy, whether collaboratively or non-collaboratively [30], [31]. It is also possible to obtain the positions of the eNodeBs from a database. Therefore, this paper assumes that the position of the eNodeBs are known to the receiver *a priori*.

In LTE systems, the number of eNodeBs in the environment for a specific network provider could be one or more depending on the number of users in the environment. Besides, when the received signal from one eNodeB has significantly high C/N_0 compared to the other eNodeBs, the received signals with low C/N_0 may not be detectable due to the near-far effect. In the position estimation problem with LTE signals, there are $2 + U$ unknowns (the receiver's horizontal position and the difference between the receiver's clock bias and each of the U eNodeBs' clock biases) and $2U - 1$ equations (U pseudoranges and $U - 1$ azimuth angle differences). It is worth mentioning that since the orientation of the antenna array is not necessarily known by the receiver, the differences of the estimated azimuth angles is used as DOA measurements. Therefore, to estimate the receiver's position and difference between its clock bias and the eNodeBs' clock biases through a static estimator (e.g., a nonlinear least-squares), measurements to at least 3 eNodeBs must be made. To increase the number of measurements, the receiver must listen to different carrier frequencies used by different LTE providers. Using a higher number of eNodeBs' measurements improves the geometric diversity, and as a result will improve the estimation accuracy. One approach to listen to multiple carrier frequencies is to use multiple antenna arrays. However, since antenna arrays are large structures, using multiple antenna arrays may not be practical for certain applications (e.g., small handheld devices).

To overcome this problem, a navigation framework based on an EKF that employs only one antenna array is proposed next.

The proposed navigation framework consists of two stages: (1) initial navigation solution for a stationary receiver on cold-start and (2) real-time navigation solution for a mobile receiver, which are discussed next.

B. Initial Navigation Solution

In the initialization stage, the estimated TOA and DOA are used to initialize the receiver's position as well as the difference between the receiver's clock bias and each of the eNodeBs' clock biases and the difference between the receiver's clock drift and each of the eNodeBs' clock drifts. In order to make measurements on more eNodeBs, the stationary receiver listens to different carrier frequencies sequentially. Then, it uses the measurements obtained from all eNodeBs to estimate the state vector, defined as

$$\boldsymbol{x} \triangleq \left[\boldsymbol{r}_r^\mathsf{T}, \boldsymbol{x}_{\text{clk}_1}^\mathsf{T}, \cdots, \boldsymbol{x}_{\text{clk}_U}^\mathsf{T}\right]^\mathsf{T}, \quad (12)$$

where $\boldsymbol{r}_r \triangleq [x_r, y_r]^\mathsf{T}$ is the receiver's position vector in the xy-plane and

$$\boldsymbol{x}_{\text{clk}_u} = \left[\Delta\delta t_u, \Delta\dot{\delta} t_u\right]^\mathsf{T},$$

where $\Delta\delta t_u \triangleq \delta t_r - \delta t_s^{(u)}$; $\Delta\dot{\delta} t_u \triangleq \dot{\delta} t_r - \dot{\delta} t_s^{(u)}$; and $\dot{\delta} t_r$ and $\dot{\delta} t_s^{(u)}$ are the clock drift of the receiver and the u-th eNodeB, respectively. The system's dynamics can be modeled as

$$\boldsymbol{x}(k+1) = \mathbf{F}\boldsymbol{x}(k) + \boldsymbol{w}(k),$$

$$\mathbf{F} = \begin{bmatrix} \mathbf{I}_2 & \mathbf{0}_{2\times 2U} \\ \mathbf{0}_{2U\times 2} & \mathbf{F}_{\text{clk}} \end{bmatrix},$$

$$\mathbf{F}_{\text{clk}} = \text{diag}\left[\mathbf{F}_{\text{clk}_1}, \ldots, \mathbf{F}_{\text{clk}_U}\right], \qquad \mathbf{F}_{\text{clk}_u} = \begin{bmatrix} 1 & T_{sub} \\ 0 & 1 \end{bmatrix},$$

where $\mathbf{I}_m$ is identity matrix of size m; $\mathbf{0}_{m\times n}$ is an $m \times n$ matrix of zeros; T_{sub} is the sampling period, which is assumed to be one LTE frame length; and $\boldsymbol{w}(k) = [\mathbf{0}_{1\times 2}, \boldsymbol{w}_{\text{clk}}(k)^\mathsf{T}]^\mathsf{T}$ and $\boldsymbol{w}_{\text{clk}}(k)$ is a discrete-time zero-mean white noise sequence with covariance $\mathbf{Q}_{\text{clk}}$ given by

$$\mathbf{Q}_{\text{clk}} = \begin{bmatrix} \mathbf{Q}_{\text{clk}_1} & \mathbf{Q}_{\text{clk}_r} & \cdots & \mathbf{Q}_{\text{clk}_r} \\ \mathbf{Q}_{\text{clk}_r} & \mathbf{Q}_{\text{clk}_2} & \cdots & \mathbf{Q}_{\text{clk}_r} \\ \vdots & \vdots & \ddots & \vdots \\ \mathbf{Q}_{\text{clk}_r} & \mathbf{Q}_{\text{clk}_r} & \cdots & \mathbf{Q}_{\text{clk}_U} \end{bmatrix},$$

where $\mathbf{Q}_{\text{clk}_r}$ and $\{\mathbf{Q}_{\text{clk}_u}\}_{u=1}^U$ are defined as

$$\mathbf{Q}_{\text{clk}_u} \triangleq \mathbf{Q}_{\text{clk}_r} + \mathbf{Q}_{\text{clk}_{s_u}},$$

$$\mathbf{Q}_{\text{clk}_r} = \begin{bmatrix} S_{\tilde{w}_{\delta t_r}} T_{sub} + S_{\tilde{w}_{\dot{\delta} t_r}} \frac{T_{sub}^3}{3} & S_{\tilde{w}_{\dot{\delta} t_r}} \frac{T_{sub}^2}{2} \\ S_{\tilde{w}_{\dot{\delta} t_r}} \frac{T_{sub}^2}{2} & S_{\tilde{w}_{\dot{\delta} t_r}} T_{sub} \end{bmatrix},$$

where $S_{\tilde{w}_{\delta t_r}}$ and $S_{\tilde{w}_{\dot{\delta} t_r}}$ are the receiver's clock bias and drift process noise power spectra, respectively, and $\mathbf{Q}_{\text{clk}_{s_u}}$ has a structure similar to $\mathbf{Q}_{\text{clk}_r}$, except that $S_{\tilde{w}_{\delta t_r}}$ and $S_{\tilde{w}_{\dot{\delta} t_r}}$ are replaced with $S_{\tilde{w}_{\delta t_{s_u}}}$ and $S_{\tilde{w}_{\dot{\delta} t_{s_u}}}$, respectively.

The measurement vector is defined as

$$z \triangleq h(x) + v = \begin{bmatrix} \rho \\ \phi \end{bmatrix},$$

where

$$\rho = \left[\rho^{(0)}, \cdots, \rho^{(U-1)} \right]^{\mathsf{T}},$$

$$\phi = \left[\Delta\phi^{(1)}, \cdots, \Delta\phi^{(U-1)} \right]^{\mathsf{T}}, \quad \text{for } \Delta\phi^{(u)} \in [-\pi, \pi],$$

where $\Delta\phi^{(u)} \triangleq \phi_{LOS}^{(u)} - \phi_{LOS}^{(0)}$ and v is the measurement noise, which is modeled as zero-mean white noise sequence with covariance matrix defined as

$$\mathbf{R} = \begin{bmatrix} \mathbf{R}_{\mathrm{TOA}} & \mathbf{0}_{U \times U} \\ \mathbf{0}_{U-1 \times U} & \mathbf{R}_{\mathrm{DOA}} \end{bmatrix}, \tag{13}$$

where $\mathbf{R}_{\mathrm{TOA}} = \mathrm{diag}\left[\sigma_\rho^{(0)\,2}, \cdots, \sigma_\rho^{(U-1)\,2} \right]$ and $\mathbf{R}_{\mathrm{DOA}}$ is given by

$$\mathbf{R}_{\mathrm{DOA}} = \begin{bmatrix} \sigma_{\phi,1}^{\,2} & \sigma_\phi^{(0)\,2} & \cdots & \sigma_\phi^{(0)\,2} \\ \sigma_\phi^{(0)\,2} & \sigma_{\phi,2}^{\,2} & \cdots & \sigma_\phi^{(0)\,2} \\ \vdots & \vdots & \ddots & \vdots \\ \sigma_\phi^{(0)\,2} & \sigma_\phi^{(0)\,2} & \cdots & \sigma_{\phi,U-1}^{\,2} \end{bmatrix},$$

where $\sigma_{\phi,i}^{\,2} = \sigma_\phi^{(0)\,2} + \sigma_\phi^{(i)\,2}$.

C. Real-Time Navigation

In the real-time navigation stage, only the TOA measurements are used. Therefore, different antenna elements can be used to listen to different carrier frequencies pertaining to different eNodeBs in the environment. Using the LTE SDRs proposed in the literature, it is possible to obtain pseudoranges to each eNodeB in the environment [7]–[9], [13]. To navigate with obtained pseudoranges, proposed approaches in the literature either: (1) modeled $\Delta\delta t_u$ as a linear function, whose parameters were calculated by post-processing the data [10], (2) assumed the receiver to have access to estimates of its own clocks for all time (e.g., from GPS signals), enabling the receiver to estimate $\Delta\delta t_u$ in a post processing fashion [8], or (3) assumed the availability of the receiver's states $r_r(0)$, $\dot{r}_r(0)$, $\delta t_r(0)$, and $\dot{\delta t}_r(0)$ (e.g., from GPS signals), which are used to initialize the EKF [13], [14]. These approaches suffer from the following shortcomings: (1) they use a crude estimate of the clock bias time evolution (approach 1), (2) they are not real-time (approaches 1 and 2), and (3) they do not produce a navigation solution on cold-start without access to GPS (approaches 2 and 3). In contrast, the initial navigation solution produced in the first stage resolves all such shortcomings, as it produces a navigation solution without GPS, which could be subsequently used to initialize the EKF for real-time navigation. Note that this stage utilizes TOA measurements which are significantly more precise than DOA measurements, making them more favorable to produce a real-time navigation solution for a mobile receiver.

VI. SIMULATION RESULTS

In this section, the accuracy of the proposed method is evaluated through numerical simulations. First, the estimated TOA and DOA is analyzed in a multipath environment and for different setups. Next, the accuracy of the position estimate obtained using the proposed framework is evaluated.

A. Joint TOA and DOA Estimation Performance

In this subsection, the accuracy of joint TOA and DOA estimation in a multipath environment is evaluated for three scenarios: (1) a fixed number of antennas and transmission bandwidth while varying the C/N_0, (2) a fixed C/N_0 and transmission bandwidth while varying the number of antennas, and (3) a fixed C/N_0 and number of antennas while varying the bandwidth. The received signal impinging the antenna array was set to have one LOS and one multipath component with the characteristics shown in Table II. For each scenario, the actual CFR (cf. (2)) was first generated without any noise based on the number of antennas, the transmission bandwidth, and the multipath characteristics shown in Table II. Then, 10^3 white Gaussian noise realizations were generated for each CFR and 10^3 CFR estimates were subsequently obtained by adding each noise realization to the actual CFR. The noise variance was assigned such that the predetermined C/N_0 for each case of every scenario was achieved. The TOA and DOA estimates were obtained using the approach discussed in Section IV for each of the CFR estimates. The root mean squared-error (RMSE) of the 10^3 TOA and DOA estimates was calculated for each case of each scenario. The parameters M, P, K, and R were set to $M \equiv N$, $P \equiv K \equiv M/2 + 1$, and $R \equiv 20$.

TABLE II
RECEIVED SIGNAL CHARACTERISTICS AT THE ANTENNA ARRAY

	α	τ	θ	ϕ
LOS	1	1×10^{-8}	$45°$	$30°$
Multipath	0.5	20×10^{-8}	$35°$	$40°$

First, the number of antennas was assigned to $M = 4$ and the transmission bandwidth was assumed to be 10 MHz. Fig. 3 shows the RMSE of the estimated TOA and DOA for different C/N_0.

Second, the transmission bandwidth was set to 10 MHz and the C/N_0 to 60 dB-Hz. Then, the RMSE of TOA and DOA estimates were obtained for different number of antennas. Fig. 4 shows the RMSE of the TOA and DOA estimates for different M.

Third, the number of antennas was set to $M = 4$ and $C/N_0 = 60$ dB-Hz. The RMSE of the TOA and DOA estimates for different LTE transmission bandwidths were obtained.

The following remarks may be concluded from Fig. 3–5.

Remark 1 Increasing C/N_0 helps differentiate the signal subspace from the noise subspace. As a result, the TOA and DOA estimation accuracy is improved, as shown in Fig. 3.
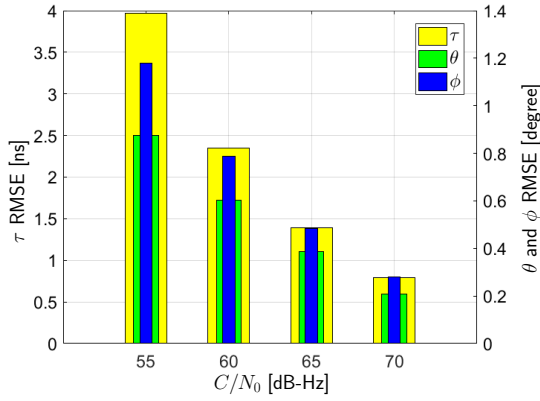
Fig. 3. Joint TOA and DOA estimation performance for different C/N_0. Here, $M = N = 4$ and the bandwidth was set to 10 MHz.
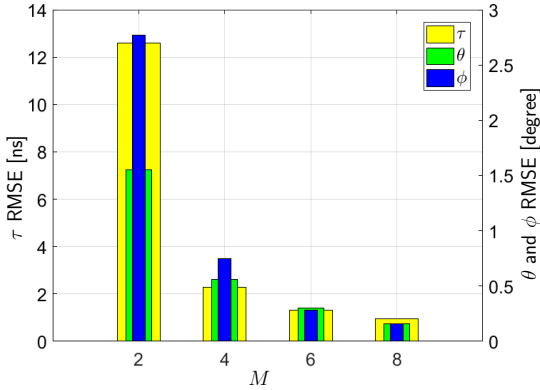

Fig. 4. Joint TOA and DOA estimation performance for different M. Here, $C/N_0 = 60$ dB-Hz and the bandwidth was set to 10 MHz.
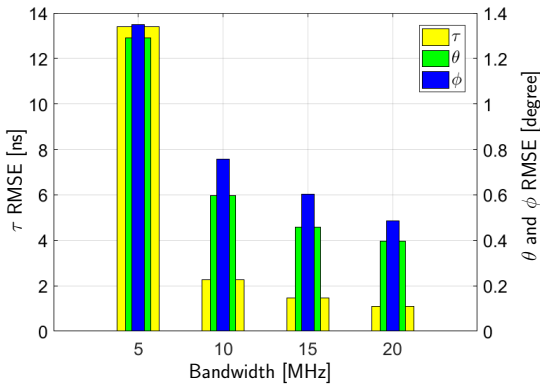

Fig. 5. Joint TOA and DOA estimation performance for different LTE transmission bandwidths. Here, $C/N_0 = 60$ dB-Hz and $M = 4$.

More importantly, it can be seen that C/N_0 has approximately the same effect on the TOA and DOA estimation accuracies.

Remark 2 Fig. 4 shows that M has approximately the same effect on the TOA and DOA estimation accuracies. Therefore, for small bandwidths, it is possible to improve the estimation accuracy by increasing the number of antennas. However, it is shown in [23] that for large bandwidths, the estimation accuracy improvement becomes negligible when M increases.

Remark 3 Increasing the bandwidth helps differentiate the LOS signal from multipath. As a result, the TOA and DOA

estimation accuracy is improved, as shown in Fig. 5. It can also be seen that the bandwidth has more effect on the TOA estimation accuracy than on the DOA estimation accuracy.

B. Initial Navigation Solution Performance

In this subsection, the accuracy of the proposed framework for estimating $\boldsymbol{x}$ defined in (12) for a stationary receiver on cold start is evaluated. It was assumed that a receiver with an antenna array of $M = N = 2$ was located at $\boldsymbol{r}_r$, which was chosen randomly in an environment surrounded by eNodeBs. The receiver was listening to 3 eNodeBs, which were placed on a circle centered at the origin with radius 1000 m. The eNodeBs were assumed to be uniformly separated on the circle and had the same height of 20 m as depicted in Fig. 6. The transmission bandwidth was assumed to be 5 MHz and $C/N_0 = 60$ dB-Hz. The transmission channel was assumed to have the LOS signal and only one multipath component with $\alpha = 0.5$ and $\phi = 40°$. Using the same approach discussed in Section VI-A, 10^3 CFR estimates were generated based on the number of antennas, transmission bandwidth, received signal's C/N_0, and multipath characteristics. Then, the standard deviations of the resulting TOA and DOA estimates over time were calculated. These standard deviations were found to be $\sigma_\tau = 44.2$ ns and $\sigma_\phi = 4.42°$ for TOA and DOA, respectively. The receiver's clock oscillator was modeled as a temperature-compensated crystal oscillator (TCXO) with $S_{\tilde{w}_{\delta t_r}} \approx h_{0,r}/2$ and $S_{\tilde{w}_{\delta t_r}} \approx 2\pi^2 h_{-2,r}$, where $h_{0,r} = 9.4 \times 10^{-20}$ and $h_{-2,r} = 3.8 \times 10^{-21}$. The eNodeBs' clock oscillators were modeled as oven-controlled crystal oscillators (OCXOs) with $S_{\tilde{w}_{\delta t_{s_i}}} \approx h_{0,s}/2$ and $S_{\tilde{w}_{\delta t_{s_i}}} \approx 2\pi^2 h_{-2,s}$, where $h_{0,s} = 8 \times 10^{-20}$ and $h_{-2,s} = 4 \times 10^{-23}$.
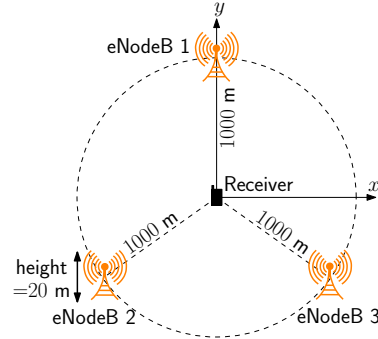

Fig. 6. Environmental layout of the simulation setup. The receiver was listening to 3 eNodeBs, which were placed uniformly on a circle centered at the origin with radius 1000 m. The height of the eNodeBs were assumed to be 20 m.

TOA and DOA measurements were generated for all the eNodeBs using the above settings for 20 s. The EKF's initial estimate was obtained from $\hat{\boldsymbol{x}}(0|-1) \sim \mathcal{N}[\boldsymbol{0}_{8\times1}, \mathbf{P}(0|-1)]$ with the initial estimation error covariance $\mathbf{P}(0|-1) = \text{diag}[10^6, 10^6, 10^8, 1, 10^8, 1, 10^8, 1]$. Fig. 7(a)-(b) show the x and y position estimation error and their associated 3σ bounds for one EKF run. Fig. 7(c)-(h) show the estimation error of the differences between the receiver clock bias and drift with those of each of the eNodeBs and their associated 3σ bounds

for one EKF run. Then, 10^3 EKF runs were performed with different EKF initial estimate $\hat{\boldsymbol{x}}(0|-1)$ and different process noise $\boldsymbol{w}$ and measurement noise $\boldsymbol{v}$ realizations in each run. The average final positioning error after 20 seconds was calculated to be 1.21 m.
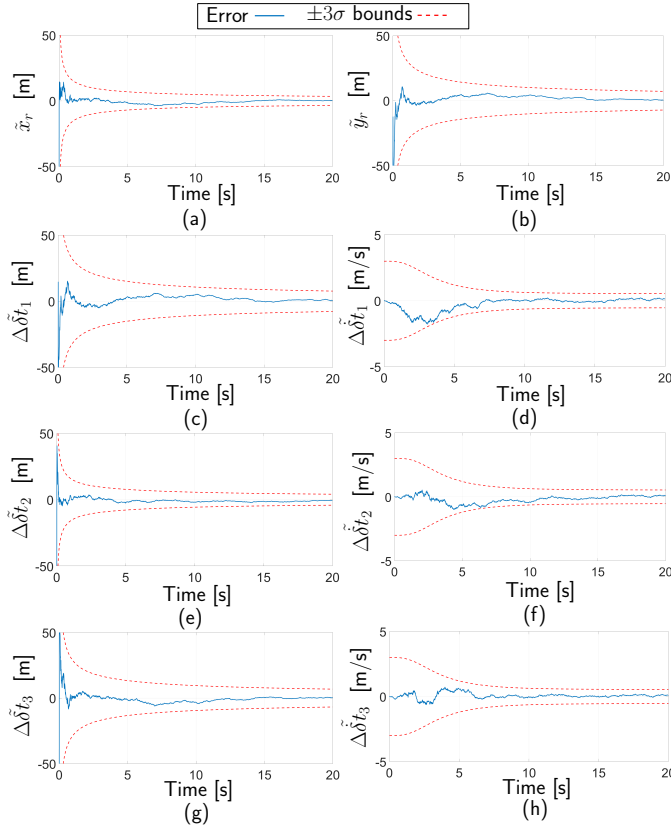

Fig. 7. The receiver's (a) x and (b) y position estimation errors and their associated 3σ bounds

VII. Experimental Results

To evaluate the performance of the proposed framework, a field test was conducted with real LTE signals in a semi-urban environment. In this section, the experimental setup and results are provided.

A. Experimental Setup

To perform the experiment, a ground vehicle was equipped with

- Four consumer-grade 800/1900 MHz cellular omnidirectional antennas to record LTE signals. The antennas were arranged in a 2×2 UPA array structure with $d = 7$ cm.
- Four National Instruments (NI) single-channel universal software radio peripherals (USRPs) whose local oscillators were synchronized using OctoClock-G CDA-2990 (an 8-channel external reference clock). The USRPs were used to simultaneously down-mix and synchronously sample the LTE signals received by the four antennas.
- An ethernet switch to connect to the USRPs and store the LTE signal samples on a host laptop computer for post-processing.

- A USRP to transmit a tone signal before performing the experiment to remove the phase offsets between the USRPs.
- A USRP to sample GPS signals for ground truth.
- A host laptop computer to store the data for post-processing.
- A GPS antenna to discipline the OctoClock's oscillator and to sample GPS signals from which the "ground truth" navigation solution is obtained.

Fig. 8 shows the experimental setup. Since the signals were stored for post-processing, the sampling rate had to be decreased to overcome data overflow problems. In this experimental setup with a 2×2 antenna array, the sampling rate was set to 5 Msps. For a higher number of antennas, this rate needs to be decreased or an ethernet switch that supports high data rates must be used instead. It is worth mentioning that by implementing the proposed receiver in hardware (e.g., digital signal processors (DSPs) and field-programmable gate arrays (FPGAs)), the sampling rate and number of antennas could be increased, which will improve the estimation accuracy (see simulation results analysis in Section VI). However, increasing the number of antennas will increase the size of the structure, which could be impractical for some platforms (e.g., handheld devices).
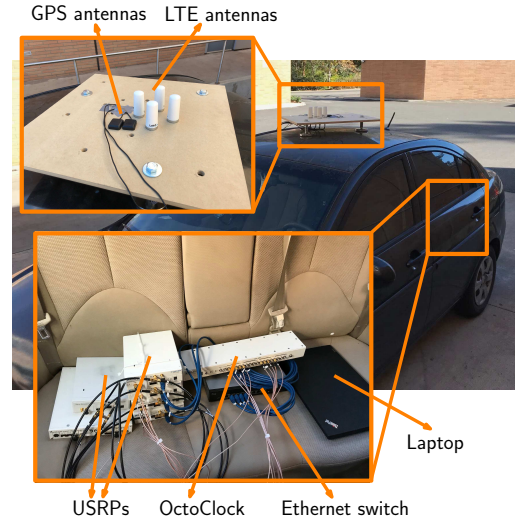

Fig. 8. Experimental hardware setup. A ground vehicle was equipped with: (1) four LTE antennas arranged in a 2×2 UPA structure to receive LTE signals, (2) GPS antennas to discipline the clock of the OctoClock and be used as the "ground truth", (3) USRPs to receive LTE and GPS signals (4) OctoClock to synchronize the USRPs. The signals were recorded in a laptop computer for post-processing.

B. Calibration

It was mentioned in Section VII-A that an OctoClock was used to synchronize the oscillators of all USRPs. However, other components aside from the local oscillators may contribute to a phase error between the USRPs, including: filters, mixers, amplifiers, and phase locked-loops in the USRPs. These factors may vary with time, temperature, and mechan-

ical conditions. To remove these errors, initial and periodic calibration is required [32].

To calibrate the USRPs, a calibration tone must be transmitted to all USRPs using matched-length radio frequency (RF) cables. Then, the phase and amplitude differences between all the USRPs with a reference USRP, which is chosen to be the first USRP, must be measured. The phase and amplitude difference must be removed from the received signals over the course of the experiment. Since the phase differences may vary with time and temperature, it is important to perform the calibration routine before each experiment.

Fig. 9 shows the in-phase components of the received signals for four USRPs, each of which was connected to the USRP transmitting the calibration tone using matched-length RF cables. It can be seen that the received signals at the USRPs have both amplitude and phase shifts, which must be calculated and removed before the experiment.
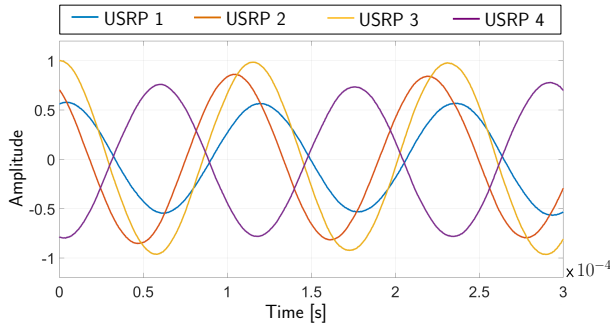

Fig. 9. In-phase components of the received tone signal at four USRPs, which were connected to the USRP transmitting the calibration tone using matched-length RF cables.

C. Experimental Results

The experiment was performed in a semi-urban environment and the vehicle-mounted receiver was stationary. LTE signals on two different LTE carrier frequencies used by the U.S. LTE cellular providers AT&T and T-Mobile were recorded sequentially at 1955 and 2145 MHz, respectively. Then, the recorded data was used to estimate the TOA and DOA of each eNodeB. Next, the position of the receiver was estimated using the navigation framework discussed in Section V.

The EKF's initial estimate was assumed to be $\hat{\boldsymbol{x}}(0|-1) = \boldsymbol{0}_{12 \times 1}$ with initial estimation error covariance of $\mathbf{P}(0|-1) = \text{diag}\left[\mathbf{P}_{0,r}, \mathbf{P}_{0,\text{clk}_1}, \cdots, \mathbf{P}_{0,\text{clk}_5}\right]$ where $\mathbf{P}_{0,r} = 10^6 \cdot \mathbf{I}_2$ and $\mathbf{P}_{0,\text{clk}_i} = \text{diag}\left[10^8, 1\right]$. Note that in many applications where there is no physical process noise (e.g., an stationary receiver's position), it is common to use an artificial process noise [33]. Therefore, the process noise covariance was assumed to be $\mathbf{Q} = \text{diag}\left[\epsilon\, \mathbf{I}_2, \mathbf{Q}_{\text{clk}}\right]$, where ϵ was set to 10^{-10} m^2. The USRPs were synchronized using an OctoClock with a GPS-disciplined oscillator. The eNodeBs' oscillators are also disciplined by GPS. Therefore, it is possible to model both the receiver's and eNodeBs' clock oscillators as OCXOs with $S_{\tilde{w}_{\delta t_r}} = S_{\tilde{w}_{\delta t_{s_i}}} \approx h_0/2$ and $S_{\tilde{w}_{\dot{\delta}t_r}} = S_{\tilde{w}_{\dot{\delta}t_{s_i}}} \approx 2\pi^2 h_{-2}$, where $h_0 = 8 \times 10^{-20}$ and $h_{-2} = 4 \times 10^{-23}$. Since the receiver was stationary, the TOA and DOA measurements can be assumed constant over short period of time. Therefore, it is possible to divide the measurements into short period windows (e.g., 1 s), measure the variance of the estimated pseudoranges and phases, and use them to construct the measurement covariance matrix $\mathbf{R}$ as shown in (13).

The receiver had LOS to 5 eNodeBs: 4 from T-Mobile and 1 from AT&T. Fig. 10 shows the environment layout as well as the position of the eNodeBs. Fig. 11 shows the receiver's x- and y- position estimation errors and their associated 3σ, respectively. The results show a final error of 0.55 m after 15 s.
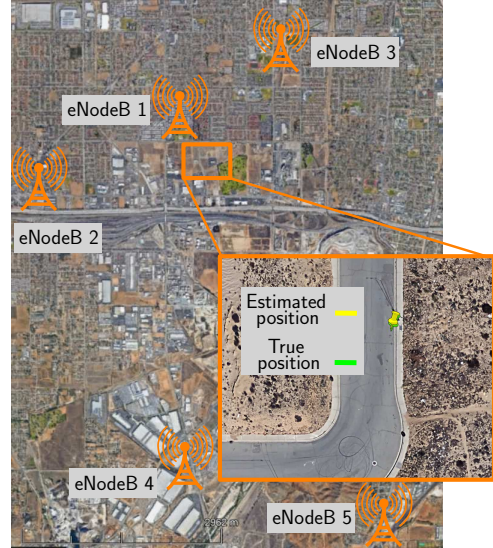

Fig. 10. Environmental layout, the positions of the eNodeBs in the environment, and the true and estimated position of the receiver. The results show a 0.55 m error in the horizontal receiver position estimate.
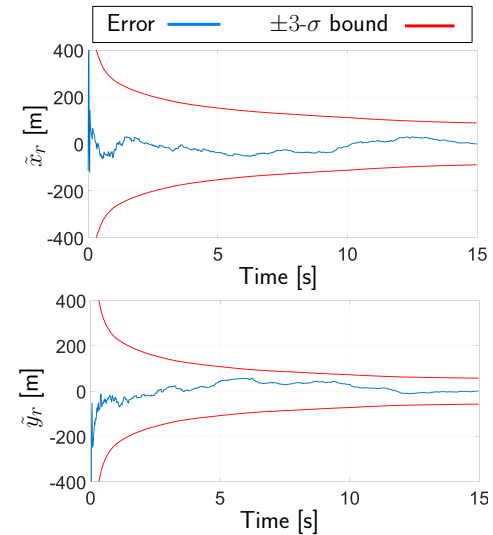

Fig. 11. The receiver's x- and y- position estimation errors for a stationary receiver and their associated 3σ bounds. The results show a final error of 0.55 m in the position estimate.

VIII. Conclusions

This paper developed an approach to jointly estimate the TOA and DOA of LTE signals. A navigation framework was proposed, which used the estimated TOA and DOA to estimate the position of the receiver, the difference between the receiver's clock bias and each LTE eNodeB, and the difference between the receiver's clock drift and each eNodeB. Unlike existing approaches in the literature for LTE-based navigation, the approach developed in this paper is capable of producing a navigation solution for the stationary receiver on cold start, without any *a priori* knowledge about the receiver's initial states. The accuracy of the estimated TOA and DOA for different transmission bandwidths, number of antennas, and C/N_0 was evaluated through simulations. Experimental results were presented showing a final error of 0.55 m in the receiver's position estimate with the proposed approach.

ACKNOWLEDGMENT

REFERENCES

[1] J. del Peral-Rosado, J. Lopez-Salcedo, G. Seco-Granados, F. Zanier, and M. Crisci, "Achievable localization accuracy of the positioning reference signal of 3GPP LTE," in *Proceedings of International Conference on Localization and GNSS*, June 2012, pp. 1–6.

[2] W. Xu, M. Huang, C. Zhu, and A. Dammann, "Maximum likelihood TOA and OTDOA estimation with first arriving path detection for 3GPP LTE system," *Transactions on Emerging Telecommunications Technologies*, vol. 27, no. 3, pp. 339–356, 2016.

[3] C. Gentner, T. Jost, W. Wang, S. Zhang, A. Dammann, and U. Fiebig, "Multipath assisted positioning with simultaneous localization and mapping," *IEEE Transactions on Wireless Communications*, vol. 15, no. 9, pp. 6104–6117, September 2016.

[4] Z. Kassas, J. Khalife, K. Shamaei, and J. Morales, "I hear, therefore I know where I am: Compensating for GNSS limitations with cellular signals," *IEEE Signal Processing Magazine*, pp. 111–124, September 2017.

[5] M. Hofer, J. McEachen, and M. Tummala, "Vulnerability analysis of LTE location services," in *Proceedings of Hawaii International Conference on System Sciences*, January 2014, pp. 5162–5166.

[6] C. Gentner, E. Munoz, M. Khider, E. Staudinger, S. Sand, and A. Dammann, "Particle filter based positioning with 3GPP-LTE in indoor environments," in *Proceedings of IEEE/ION Position, Location and Navigation Symposium*, April 2012, pp. 301–308.

[7] J. del Peral-Rosado, J. Lopez-Salcedo, G. Seco-Granados, F. Zanier, P. Crosta, R. Ioannides, and M. Crisci, "Software-defined radio LTE positioning receiver towards future hybrid localization systems," in *Proceedings of International Communication Satellite Systems Conference*, October 2013, pp. 14–17.

[8] M. Driusso, C. Marshall, M. Sabathy, F. Knutti, H. Mathis, and F. Babich, "Vehicular position tracking using LTE signals," *IEEE Transactions on Vehicular Technology*, vol. 66, no. 4, pp. 3376–3391, April 2017.

[9] K. Shamaei, J. Khalife, S. Bhattacharya, and Z. Kassas, "Computationally efficient receiver design for mitigating multipath for positioning with LTE signals," in *Proceedings of ION GNSS Conference*, September 2017, pp. 3751–3760.

[10] F. Knutti, M. Sabathy, M. Driusso, H. Mathis, and C. Marshall, "Positioning using LTE signals," in *Proceedings of Navigation Conference in Europe*, April 2015, pp. 1–8.

[11] K. Shamaei, J. Khalife, and Z. Kassas, "Comparative results for positioning with secondary synchronization signal versus cell specific reference signal in LTE systems," in *Proceedings of ION International Technical Meeting Conference*, January 2017, pp. 1256–1268.

[12] M. Driusso, F. Babich, F. Knutti, M. Sabathy, and C. Marshall, "Estimation and tracking of LTE signals time of arrival in a mobile multipath environment," in *Proceedings of International Symposium on Image and Signal Processing and Analysis*, September 2015, pp. 276–281.

[13] K. Shamaei, J. Khalife, and Z. Kassas, "Exploiting LTE signals for navigation: Theory to implementation," *IEEE Transactions on Wireless Communications*, vol. 17, no. 4, pp. 2173–2189, April 2018.

[14] Z. Kassas and T. Humphreys, "Observability analysis of collaborative opportunistic navigation with pseudorange measurements," *IEEE Transactions on Intelligent Transportation Systems*, vol. 15, no. 1, pp. 260–273, February 2014.

[15] M. Vanderveen, C. Papadias, and A. Paulraj, "Joint angle and delay estimation (JADE) for multipath signals arriving at an antenna array," *IEEE Communications Letters*, vol. 1, no. 1, pp. 12–14, January 1997.

[16] M. Vanderveen, A. V. der Veen, and Paulraj, "Estimation of multipath parameters in wireless communications," *IEEE Transactions on Signal Processing*, vol. 46, no. 3, pp. 682–690, March 1998.

[17] R. Schmidt, "Multiple emitter location and signal parameter estimation," *IEEE Transactions on Antennas and Propagation*, vol. 34, no. 3, pp. 276–280, March 1986.

[18] R. Roy and T. Kailath, "ESPRIT-estimation of signal parameters via rotational invariance techniques," *IEEE Transactions on Acoustics, Speech, and Signal Processing*, vol. 37, no. 7, pp. 984–995, July 1989.

[19] T. Shan, M. Wax, and T. Kailath, "On spatial smoothing for direction-of-arrival estimation of coherent signals," *IEEE Transactions on Acoustics, Speech, and Signal Processing*, vol. 33, no. 4, pp. 806–811, August 1985.

[20] Y. Hua and T. Sarkar, "Matrix pencil method for estimating parameters of exponentially damped/undamped sinusoids in noise," *IEEE Transactions on Acoustics, Speech, and Signal Processing*, vol. 38, no. 5, pp. 814–824, May 1990.

[21] Y. Hua, "Estimating two-dimensional frequencies by matrix enhancement and matrix pencil," *IEEE Transactions on Signal Processing*, vol. 40, no. 9, pp. 2267–2280, September 1992.

[22] M. Navarro and M. Najar, "TOA and DOA estimation for positioning and tracking in IR-UWB," in *Proceedings of IEEE International Conference on Ultra-Wideband*, September 2007, pp. 574–579.

[23] A. Gaber and A. Omar, "A study of wireless indoor positioning based on joint TDOA and DOA estimation using 2-D matrix pencil algorithms and IEEE 802.11ac," *IEEE Transactions on Wireless Communications*, vol. 14, no. 5, pp. 2440–2454, May 2015.

[24] 3GPP, "Evolved universal terrestrial radio access (E-UTRA); physical channels and modulation," 3rd Generation Partnership Project (3GPP), TS 36.211, January 2011. [Online]. Available: http://www.3gpp.org/ftp/Specs/html-info/36211.htm

[25] 3GPP, "Evolved universal terrestrial radio access (E-UTRA); multiplexing and channel coding," 3rd Generation Partnership Project (3GPP), TS 36.212, January 2010. [Online]. Available: http://www.3gpp.org/ftp/Specs/html-info/36212.htm

[26] H. Krim and M. Viberg, "Two decades of array signal processing research: the parametric approach," *IEEE Signal Processing Magazine*, vol. 13, no. 4, pp. 67–94, July 1996.

[27] K. Shamaei, J. Khalife, and Z. Kassas, "Performance characterization of positioning in LTE systems," in *Proceedings of ION GNSS Conference*, September 2016, pp. 2262–2270.

[28] N. Yilmazer, R. Fernandez-Recio, and T. Sarkar, "Matrix pencil method for simultaneously estimating azimuth and elevation angles of arrival along with the frequency of the incoming signals," *Digital Signal Processing*, vol. 16, no. 6, pp. 796–816, November 2006.

[29] M. Wax and T. Kailath, "Detection of signals by information theoretic criteria," *IEEE Transactions on Acoustics, Speech, and Signal Processing*, vol. 33, no. 2, pp. 387–392, April 1985.

[30] Z. Kassas, V. Ghadiok, and T. Humphreys, "Adaptive estimation of signals of opportunity," in *Proceedings of ION GNSS Conference*, September 2014, pp. 1679–1689.

[31] J. Morales and Z. Kassas, "Optimal collaborative mapping of terrestrial transmitters: receiver placement and performance characterization," *IEEE Transactions on Aerospace and Electronic Systems*, vol. 54, no. 2, pp. 992–1007, April 2018.

[32] Synchronization and MIMO capability with USRP devices. [Online]. Available: https://kb.ettus.com/Synchronization and MIMO Capability with USRP Devices

[33] Y. Bar-Shalom, X. Li, and T. Kirubarajan, *Estimation with Applications to Tracking and Navigation*. New York, NY: John Wiley & Sons, 2002.